Metalation of the Amyotrophic Lateral Sclerosis Mutant Glycine 37 to Arginine Superoxide Dismutase (SOD1) Apoprotein Restores Its Structural and Dynamical Properties in Solution to Those of Metalated Wild-Type SOD1†

Lucia Banci,[‡,§,||] Ivano Bertini,*[,‡,§] Nicola D'Amelio,[‡,#] Elisa Libralesso,[‡] Paola Turano,[‡,§] and Joan Selverstone Valentine*[,⊥]

Magnetic Resonance Center, University of Florence, Via Luigi Sacconi 6, 50019 Sesto Fiorentino, Italy, Department of Chemistry, University of Florence, Via Della Lastruccia 5, 50019 Sesto Fiorentino, Italy, FiorGen Foundation, Via Luigi Sacconi 6, 50019 Sesto Fiorentino, Florence, Italy, and Department of Chemistry and Biochemistry, University of California Los Angeles, Los Angeles, California 90095-1569

Received April 2, 2007; Revised Manuscript Received June 27, 2007

ABSTRACT: The G37R copper−zinc superoxide dismutase (SOD1) is one of the many mutant SOD1 proteins known to cause familial amyotrophic lateral sclerosis by an unknown mechanism. This particular mutation occurs in the β barrel plug, a region proposed to be critical for the structural stability of the protein. The behavior of G37R asSOD1 was studied in solution where it was observed that, when the protein is fully metalated, its global structure, mobility, and stability are virtually indistinguishable from those of the nonmutated protein. By contrast, although the presence of the G37R mutation does not result in a substantial change of the overall structure of the metal-free apoprotein in solution, it does affect the key conformational features of the β-barrel plug such that (i) apo G37R asSOD1 melts at a temperature approximately 10 °C lower than apo asSOD1, (ii) it aggregates more rapidly than apo asSOD1, and (iii) interaction with trifluoroethanol (TFE) can deform it into a structure with a much higher degree of α-helical content. The increased plasticity of the apo G37R asSOD1 mutant protein is likely responsible for its enhanced tendency to aggregate in concentrated solutions. These results suggest further that it is the metal-free apo forms of the mutant SOD1 protein that are the agents of its toxicity.

Amyotrophic lateral sclerosis (ALS)[1] is a fatal neurodegenerative disease that specifically targets motor neurons. The inherited form of the disease, familial ALS (fALS), has been linked to mutations in several different genes, the best characterized of which is the *sod1* gene, which codes for the enzyme copper−zinc superoxide dismutase (SOD1). Wild-type SOD1 (wtSOD1) is a homodimeric protein, each subunit of which binds one copper and one zinc ion and contains an intramolecular disulfide bond. Over 100 different ALS-causing mutations in the SOD1 gene have been reported to date (see www.alsod.org), and the properties of many of the resulting mutant SOD1 proteins (mutSOD1s) have been studied and compared in cell culture, transgenic mice, and isolated mutSOD1 in an effort to determine the nature of their toxicities to motor neurons (*1*, *2*).

It is well-established that SOD1-linked ALS is caused by a gain of function mechanism in which mutSOD1s have become toxic as a consequence of the mutations. Although the exact nature of the toxicity is as yet unknown, a growing body of evidence suggests that mutSOD1 misfolding and oligomerization are involved (*3*, *4*). However it is not known whether the toxic forms of the mutant SOD1 proteins contain metal ions or have ever been metalated by copper or zinc or whether they have in some way been covalently modified on the pathway to toxicity.

Biophysical studies of isolated mutSOD1s have uncovered a surprisingly wide diversity of properties for the different mutSOD1s (*5*). There are several mutSOD1s with mutations in either of the two loops that comprise the metal binding region, for example, S134N or H46R, that have dramatically

† This work was supported in part by MIUR PRIN-2005 2005039878, MIUR FIRB RBLA032ZM7 and FIRB RBNE03PX83, by European Union Contract LSHG-CT-2004-512052 "UPMAN-Understanding Protein Misfolding and Aggregation by NMR", and NIH Grant NS049134 (to J.S.V.).

* To whom correspondence may be addressed. Ivano Bertini: e-mail ivanobertini@cerm.unifi.it; phone +39 055 4574270; fax +39 055 4574271. Joan Selverstone Valentine: e-mail jsv@chem.ucla.edu; phone +1 310 8259835; fax +1 310 2069880.

‡ Magnetic Resonance Center, University of Florence.

§ Department of Chemistry, University of Florence.

|| FiorGen Foundation.

Recipient of a fellowship provided by Consorzio Interuniversitario per le Risonanze Magnetiche di Metalloproteine Paramagnetiche.

⊥ University of California Los Angeles.

[1] Abbreviations: asSOD, superoxide dismutase in which Cys6 and Cys111 have been mutated to alanine and serine, respectively; ALS, amyotrophic lateral sclerosis; BSA, bovine serum albumin; CCD, charge-coupled device; EPR, electron paramagnetic resonance; fALS, familial amyotrophic lateral sclerosis; FFCR, fast-field cycling relaxometry; HSQC, heteronuclear single quantum coherence; ICP, inductively coupled plasma; INEPT, insensitive nuclei enhanced by polarization transfer; mutSOD1, mutant SOD1 protein; NMR, nuclear magnetic resonance; NMRD, nuclear magnetic relaxation dispersion; NOE, nuclear Overhauser effect; NOESY, nuclear Overhauser effect spectroscopy; PCR, polymerase chain reaction; R_1, longitudinal relaxation rate; R_2, transversal relaxation rate; rmsd, root mean square deviation; SOD1, superoxide dismutase; TFE, trifluoroethanol; WATERGATE, water suppression by gradient-tailored excitation; wt, wild-type.

10.1021/bi700620r CCC: $37.00
Published on Web 08/07/2007

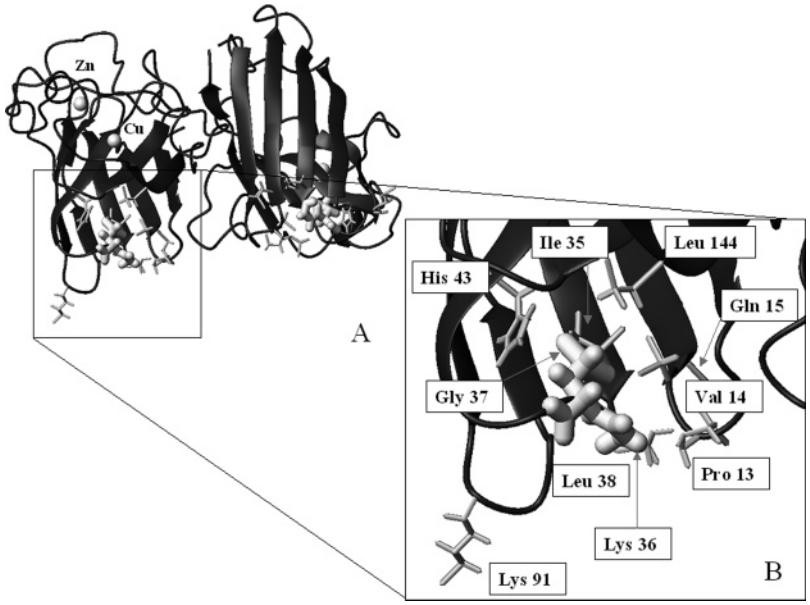

FIGURE 1: (A) The structure of asSOD1. (B) Enlargement of the plug region. The native Gly37 and the plug residue Leu38 are shown as sticks. Important residues defining the plug region in the vicinity of the mutation are shown as wireframe.

altered metal binding and other biophysical properties and that crystallize in filamentous arrays (*6*, *7*). There are several other mutSOD1s with mutations remote from the metal binding region, for example, A4V or G37R, that bind metal ions relatively normally and that, in their metalated forms, have SOD activities, crystal structures, and stabilities very similar or identical to metalated wtSOD1 (*8*−*10*). Likewise, the apoproteins derived from mutSOD1s cover a wide range of properties. Some are extremely destabilized, and others are actually more stable relative to the wtSOD1 apoprotein (*11*).

By contrast, when expressed in cell culture or in transgenic mice, the apparently diverse mutSOD1s appear to be much more similar to each other and different from wtSOD1 in their toxicities and other biological effects. For example, abnormal protein deposits containing precipitated mutSOD1 are found in neural tissue for the many different strains of SOD1-ALS transgenic mice, while the mice expressing human wtSOD1 at high levels show no such deposits (*12*). In a cell culture aggregation assay developed by Wang et al. (*13*), expression of each of 13 highly diverse mutSOD1s, but not wtSOD1, caused them to form sedimentable structures with poor detergent solubility. In another cell culture model system using motor neuronal cells, Ferri et al. (*14*) found that 12 highly diverse mutSOD1s, but not wtSOD1, associated with the mitochondria and shifted the redox potential within that organelle.

NMR is a powerful technique for elucidation of the structural and dynamical properties of biological macromolecules in solution, often providing information that is complementary to that obtained by X-ray crystallography. We have previously studied two mutSOD1 proteins using this technique, seeking information about properties that might be linked to their toxicities. In the case of fully metalated G93A SOD1, we found that the solution structure and the dynamics were changed very little from those of fully metalated wtSOD1; the only changes observed were in the immediate vicinity of the mutation (*15*). By contrast, fully metalated S134N showed behavior that was markedly different from that of wtSOD1, with areas of high mobility that are usually rigid in the metalated forms of SOD1, as well as evidence for intermolecular interactions in solution (*16*).

In the current study, our goal was to carry out an in-depth biophysical study of a mutant SOD1 protein in different states of metalation and in the metal-free apo state for comparison with the analogous derivatives of the wt protein. The mutant protein that we chose to study is G37R SOD1 (see Figure 1), a mutSOD1 with many properties similar to those of G93A but with the added advantage that, unlike G93A, the apoprotein can be reconstituted to either the Cu_2Zn_2 or the Zn_2Zn_2 form for direct comparison with the analogously metalated forms of wtSOD1. In addition, a crystal structure of metalated G37R SOD1 is available (*8*), and, like for G93A, there is a well-studied G37R transgenic mouse. In analogy with S134N (*16*) and G93A (*15*), we studied the "thermostable" form of the G37R SOD1 protein, that is, asSOD1, in which the two cysteine residues not involved in the intramolecular disulfide bond, Cys6 and Cys111, have been mutated to alanine and serine, respectively (*17*−*19*). These mutations ensured that any intermolecular contacts that we might observe in solution, such as those we observed in the case of S134N asSOD1, could not be due to the formation of intermolecular disulfide bonds from unintended air oxidation of the sample.

In the current study, we have found that G37R asSOD1 in two different metalated forms, that is, Cu_2Zn_2 and Zn_2Zn_2, is virtually identical to asSOD1 in all of the solution properties that have been studied, that the only structural changes are very local and confined to the area around the mutation, and that there is no evidence for areas of high mobility nor for intermolecular contacts in solution. The similar properties of the metalated wt and G37R SOD1s are in sharp contrast to the difference observed by us and by others for the apoproteins of wt and G37R SOD1, which are markedly different in structure and stability in solution (as shown by Rodriguez et al. (*11*) and present work). The observation that G37R asSOD1 and asSOD1 are very similar

in properties when metal ions are bound but behave differently and possess tendency to aggregate in their absence suggests to us that the toxic form of the mutSOD1 is likely to be metal-free. Thus, for those mutSOD1s such as A4V, G37R, G93A, or D101N, whose properties are virtually identical to wtSOD1 when they are in the fully metalated Cu_2Zn_2 state, it is likely that the toxic form is achieved either by failure to accomplish metalation *in vivo* or from enhanced degradation or demetalation pathways.

MATERIALS AND METHODS

Molecular Biology and Metal Content Characterization. The G37R mutation was introduced on the *sod1* gene by PCR mutagenesis (QuickChange mutagenesis kit, Stratagene, California) on the pPCuZnSODlI^q plasmid, encoding thermostable human CuZnSOD1 C6A C111S double mutant (asSOD). The resulting construct was sequenced to confirm the mutation. *Escherichia coli* TOPP1 strains were transformed with the obtained plasmid. The mutant protein was expressed in a fermentor (T = 37 °C pO_2 = 30%, both in complex 2×YT medium and in chemically defined M9 medium, supplemented with ^{15}N $(NH_4)_2SO_4$ when prepared for high-field NMR studies). Expression and purification were performed accordingly with well-established procedures (*20*, *21*). When needed, reduction of Cu(II) to Cu(I) was achieved by addition of 1.2−1.5 equiv of *p*-isoascorbic acid or sodium dithionite dissolved in degassed 20 mM phosphate buffer, pH 5, under reducing conditions. In order to obtain the demetalated enzymes, the copper and zinc ions were sequestered from the mutants following a known protocol (*22*).

Protein concentrations were determined by UV (ϵ_{265} = 6200 M^{-1} cm^{-1}) or by Coomassie assay (Pierce Perbio) with BSA as standard. Apo samples of G37R and asSOD1 were reconstituted by addition of dilute aqueous solutions of $CuSO_4$ or $ZnCl_2$ to the proteins in 20 mM phosphate buffer solutions at pH 5, as previously described.

Stock solutions of the proteins were stored at 4 °C for short-term use or at −20 °C.

Metal content analysis of G37R obtained from complex medium, was performed with a Spectro Ciros CCD ICP optical emission spectrometer (Spectro Analytical Instruments) combined with a Lichte nebulizer (*16*). The sample, about 60 μM, was obtained by diluting a concentrated stock of protein with MilliQ water. The introduction in the prechamber was accomplished by means of a peristaltic pump. Three wavelengths for the Zn (202, 206, and 213 nm) and three for the Cu (219, 219b, and 324 nm) were detected, each measurement being repeated three times. Standard solutions of Zn and Cu in MilliQ water in the range 10−100 μM were used for the standardization curve. The blank was registered using the protein buffer diluted as the sample.

High-Field NMR. If not otherwise indicated, the protein samples were in 20 mM phosphate buffer at pH 5.0, and the temperature was set to 298 K. ^1H monodimensional experiments were performed on Bruker Avance 900 MHz to observe histidine amide protons on asSOD1 and its G37R mutant in the apo form and in different metalation states (namely, Cu_2Zn_2 and Zn_2Zn_2). Sample concentration was 100 μM. These signals were used to monitor the protein metal uptake. Suppression of the water signal was accomplished through WATERGATE sequence (*23*), which allows a better detection of water-exchanging protons.

$^1H-^{15}N$ HSQC experiments were performed to monitor structural differences upon metalation or mutation. For the concentration dependence of chemical shifts, several ^{15}N HSQC spectra, at protein concentrations spanning from 1.5 to 0.06 mM, were collected on a Bruker Avance 800 MHz spectrometer equipped with a cryoprobe.

In order to identify the coordination state of the metal binding histidine residues, $^1H-^{15}N$ HSQC experiments were performed at 600 MHz, using INEPT delays optimized for the detection of $^2J_{NH}$ (*24*−*26*). In these experiments, the INEPT delay was set to 22 ms. A large window for the ^{15}N frequency (130 ppm) for the nitrogen was used allowing the observation of the histidine side-chain NH signals. The last set of experiments was performed at two different temperatures (298 and 308 K) and in the case of G37R also at pH 7.

^1H and ^{15}N backbone assignment of apo G37R mutant and apo asSOD1, of their Zn_2Zn_2 forms, and of the Cu_2Zn_2 form of G37R was performed though ^1H,^{15}N NOESY−HSQC spectra recorded at 900 MHz.

Relaxation experiments for mobility measurements were performed at 600 MHz on the G37R mutant as obtained from the expression system and in the Cu_2Zn_2 and Zn_2Zn_2 reconstituted forms. The pulse sequences used to obtain ^{15}N R_1 and R_2 rates and heteronuclear NOE spectra are described in the literature (*27*−*31*).

Other Spectroscopies. The electronic spectrum of G37R asSOD1 was recorded in the range 250−900 nm with protein concentrations of the order 10^{-4} M in the visible region and 10^{-5} M in the UV region. The samples were in 20 mM phosphate buffer, pH 5.

The secondary structure content of the protein as expressed, of the apo form, and of the reconstituted Cu_2Zn_2 and Zn_2Zn_2 derivatives was characterized at 298 K by circular dichroism (CD) in the wavelength range 190−250 nm, using 10−20 μM samples in 10 mM phosphate buffer. The copper coordination was characterized using a 500 μM sample in 20 mM phosphate buffer, pH 5, and recording spectra in the 250−1000 nm range. CD was also used to compare the stability of the different protein derivatives. Thermal denaturation in the 298−343 K range in the presence of 0−25% 2,2,2-trifluoroethanol (TFE) was followed in the UV region. All of the spectra were collected on a Jasco J-810 spectrophotometer equipped with a Peltier unit.

EPR spectra were recorded at 180 K on an Elexsys E500 spectrometer (Bruker), equipped with X-band microwave bridge (microwave frequency 9.45 GHz) and an ER 4131 VT unit for temperature control. One millimolar protein samples in 20 mM phosphate buffer at pH 5.0 were used.

The aggregation propensity of the mutant was compared with that of asSOD1 by studying the longitudinal water proton relaxation rates with a Stelar prototype of fast-field cycling relaxometer (FFCR, proton Larmor frequency 0.01−40 MHz), as already reported for the S134N variant (*16*). Relaxivity profiles were measured both for holo and apo forms of the mutant and of native asSOD1, immediately after the isolation of the proteins and then again after 2 weeks of incubation at room temperature. Measurements were performed at 298 K on 3 mM samples in 20 mM phosphate

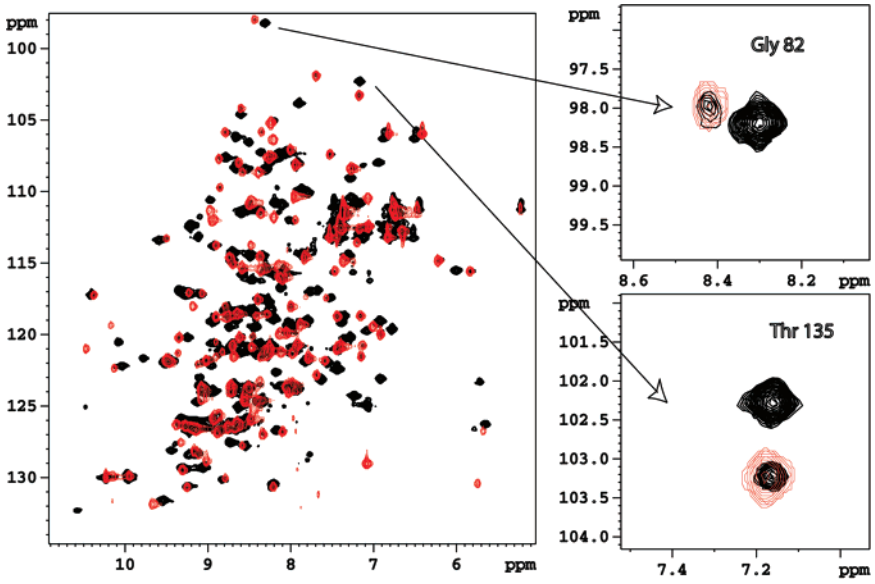

FIGURE 2: Superimposition of the ^{15}N HSQC spectra of asSOD1 (red) and its G37R mutant (black). The spectrum of the mutant presents resonance splitting for residues in the vicinity of the metal binding sites. Example are shown from Gly82 and Thr135.

buffer, pH 5.0. The holoprotein was studied in the copper(I) form to avoid paramagnetic effects.

RESULTS

Metalation State of the as Isolated Protein and Reconstitution Studies. The G37R asSOD1 protein was isolated in its dimeric form, as indicated by gel filtration (data not shown), ^{15}N NMR relaxation data, and field-dependent water relaxation rates on freshly prepared samples (see below). The binding mode of copper(II) in the copper site of G37R asSOD1, as isolated from the expression system, was characterized by EPR and visible spectroscopy and found to be virtually identical to that of copper(II) in the copper site of asSOD1.

Earlier studies in our laboratory have established that asSOD1, G93A asSOD1, and S134N asSOD1 are isolated from our expression system in the uniformly metalated Cu_2-Zn_2 form (*15*, *16*). By contrast, the G37R asSOD1 isolated from the same expression system was not. The copper and zinc content, as determined by ICP measurements, was 2.9 equiv per dimer of zinc and 0.9 of copper, indicating a relative ratio in zinc and copper content on the order of approximately 3:1, instead of the 2:2 ratio expected for a Cu_2Zn_2SOD1.

After reduction of copper(II) to copper(I) (see Material and Methods), the chemical shift values for backbone amides in the NMR ^{15}N HSQC agreed well with those of asSOD1, indicating that the overall fold of the protein did not change as a consequence of the G37R mutation. Nevertheless, resonance splitting for residues close to the metal centers was observed (Figure 2), consistent with a heterogeneous metalation state. Among the split resonances, one set was nearly identical to that of Cu_2Zn_2asSOD1.

The 1D ^{1}H NMR spectrum, tailored for the detection of imidazole NH resonances (in the region 10−16 ppm), was acquired for the G37R asSOD1 as isolated from the expression system (Figure 3A). The spectrum contained twice the number of peaks observed in the spectrum of Cu_2Zn_2asSOD1 (Figure 3B), further indicating the presence of two distinct species with structural differences in their metal binding

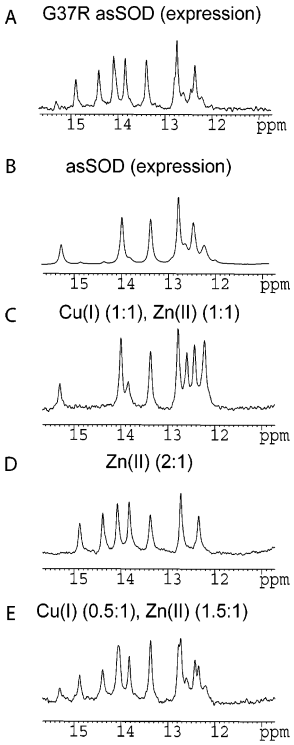

FIGURE 3: 1D ^{1}H NMR spectra tailored for the detection of imidazole NH resonances of (A) G37R as isolated from the expression system, (B) Cu_2Zn_2 asSOD1, (C) apo G37R after addition of 1.0 equiv per subunit of Zn^{2+} followed by 1.0 equiv per subunit of Cu^{2+}, (D) apo G37R after addition of 2.0 equiv per subunit of Zn^{2+}, and (E) apo G37R after addition of 1.0 equiv per subunit of Zn^{2+} followed by 0.5 equiv of Zn^{2+} and 0.5 equiv of Cu^{2+}. Because metal uptake in the copper site is slow, final spectra of the fully metalated forms have been acquired after 10 days from the addition of the last equivalent of metal ion.

regions. This observation, together with the metal stoichiometry from ICP, led us to the hypothesis that half of the subunits of the G37R protein isolated from our expression system contained zinc ions in place of copper in their copper sites.

This hypothesis was tested by reconstitution of apo G37R asSOD1 in three different ways for comparison of the

imidazole NH resonances in the 1D ^{1}H NMR: (i) by addition of 1.0 equiv per subunit of Zn^{2+} followed by 1.0 equiv per subunit of Cu^{2+}, (ii) by addition of 2.0 equiv per subunit of Zn^{2+}, and (iii) by addition of 1.0 equiv per subunit of Zn^{2+} followed by 0.5 equiv of Zn^{2+} and 0.5 equiv of Cu^{2+}. The spectra are reported in Figure 3C−E, respectively. Spectra in Figure 3C,D are typical for Cu_2Zn_2 asSOD1 and Zn_2Zn_2 asSOD1. From the comparison with Figure 3A, it clearly emerges that the protein obtained by addition of 1.5 equiv of Zn^{2+} and 0.5 of Cu^{2+} has the same spectrum as the one isolated from our expression system, although the amount of Zn_2Zn_2 (spectrum 3E) is slightly higher in the as isolated protein. The spectrum of Figure 3A can also be reproduced by adding spectrum 3C to spectrum 3D, with relative weights of the order of 1:1.

An interesting difference was observed in the zinc-binding behaviors of apo G37R asSOD1 and apo asSOD1. The first equivalent of zinc per subunit was observed to bind rapidly and stoichiometrically to give E_2Zn_2asSOD1 (E = empty) and E_2Zn_2G37RasSOD1, with no difference apparent between the behaviors of the two proteins. By contrast, addition of the second equivalent of zinc per subunit resulted in its slow binding to the copper site (as it is the case when Cu^{2+} is added to that site) for both proteins, but in the case of asSOD1, addition of 1.5 equiv per subunit of Zn^{2+} was required to saturate the copper site completely with zinc, whereas only 1.0 equiv of zinc ion was required in the case of G37R asSOD1. We conclude that the metal binding behavior of the copper site in E_2Zn_2asSOD1 and E_2Zn_2-G37RasSOD1 are similar but not identical; however, the explanation for these differences is not immediately apparent.

NMR Characterization of as Isolated G37R asSOD1. Resonance splitting in the ^{1}H−^{15}N HSQC experiment of the Cu(I) form of G37R protein, as isolated from the expression medium, is observed for a number of residues in loop I, loop IV, loop VI, loop VII (electrostatic loop), and the C-terminal amino acids. The observed differences in chemical shift between the resonances of the two differently metalated protein forms are relative small, consistent with retention of the overall fold. Such very small changes in chemical shift do not translate into differences in NOE patterns; therefore no complete characterization of the 3D structure of the protein in the Zn_2Zn_2 form was necessary.

NOE connectivities were analyzed in detail in the region nearby the mutation (within 10 Å). The large number of long-range contacts indicates that the structure of the protein is well-defined (Figure 4). The observed cross-peaks are fully consistent with the solution structure of the native form, in terms of both NOE patterns and relative intensities, except in the region that is very close to the mutation site. The average orientation of the side chain of Arg37, the mutated residue, can be defined; the Hϵ of the guanidinium group displays NOE contacts with neighboring residues. The NOE with the amide proton of Leu38 is quite strong, while weak contacts are found with the Hα of Lys36 and the Hα of Pro13. This result implies that the two positively charged side chains (Lys36 and Arg37) are repelling each other. Such an orientation is also consistent with that found in one subunit of the X-ray structure of the mutant (*8*).

Protein mobility was studied through ^{15}N relaxation data (Figure S1, Supporting Information). Average values for R_1, R_2, and NOE were 0.63 ± 0.06 s^{-1}, 25.7 ± 3.6 s^{-1}, and 0.82 ± 0.11, respectively. Accordingly, from the ratio R_2/R_1, an average correlation time for the protein tumbling of 20.5 ± 1.9 ns was estimated, further confirming that the protein is in its dimeric state. The average relaxation parameters as well as the per residue figures are very close to those of the asSOD1 protein, thus indicating that the mutation does not affect the local mobility of the protein. This result is in sharp contrast to our earlier results for S134N asSOD1 (*16*) in which the mutation was found to cause local disorder and mobility on the sub-nanosecond time scale, which was probably responsible for the abnormal protein−protein contacts.

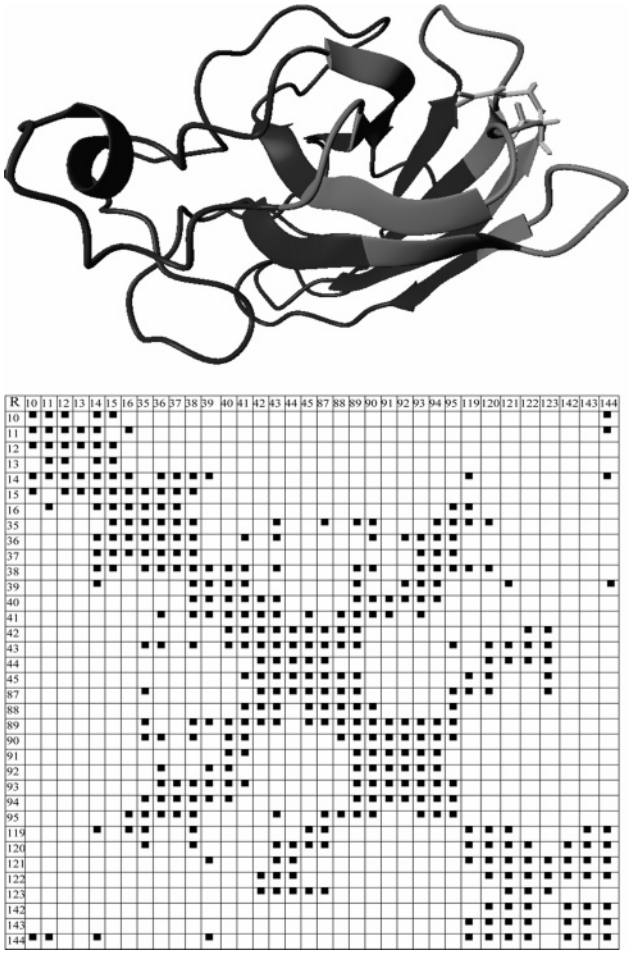

FIGURE 4: NOE contacts (■) found in the ^{1}H−^{15}N HSQC−NOESY spectrum of G37R among residues (R) belonging to the region within 0.1 nm from the mutation (light gray residues in the top image). The Arg37 side chain, shown as sticks, has been artificially inserted in the solution structure of Cu_2Zn_2 asSOD1 (pdb code 1L3N).

The superimposition of the ^{1}H−^{15}N HSQC spectra of reconstituted Cu_2Zn_2 and Zn_2Zn_2 G37R reproduces the two-dimensional map of the expressed protein, although small differences could be detected in the shift of some residues for the Cu_2Zn_2 form (90−93 and 139−142 as well as faint differences in some of the shifts of the imidazole signals of some of the copper ligands, that is, Hϵ1, Hδ2, and Hδ1 of His120 and Hϵ1 of His63).

Comparison of the Cu_2Zn_2 Forms of asSOD1 and G37R asSOD1. Detailed structural information on the reconstituted Cu_2Zn_2 G37R asSOD1 was obtained by NMR for the copper(I) diamagnetic form, by comparison of the $Cu(I)_2Zn_2$

derivatives of G37R asSOD1 and of asSOD1. $^1H-^{15}N$ HSQC spectra were used to monitor possible variations in the backbone conformation. Using the common formula ($\Delta_{av} = [(\Delta\delta_{NH}^2 + (\Delta\delta_N/5)^2)/2]^{1/2}$), the largest changes in chemical shift are observed for the mutated residue Arg37, for the plug residue Leu38, and for residues on the facing loops, that is, Gly10 and Gln15 on loop I and Lys91 on loop V.

The coordination properties of the histidine residues were followed through $^1H-^{15}N$ HSQC heteronuclear experiments optimized for the detection of the ^2J couplings between the nitrogens and the protons bound to the adjacent carbons in the imidazole ring (*24*, *32*). Spectra were acquired for the $Cu(I)_2Zn_2$ forms of G37R and asSOD1. Typically, the ^{15}N resonances of imidazoles are shifted at 160−185 ppm range if the nitrogen is protonated, at about 250 ppm if deprotonated, and in the range 200−230 ppm if deprotonated and metal bound (*24*−*26*, *33*). The assignment of the corresponding resonances is reported in the Supporting Information (Table S2); it was obtained by making reference to the available assignments of the Cu_2Zn_2asSOD1. No meaningful shift differences could be detected. Therefore we can conclude that the structure of the metal binding site is substantially unaffected in the Cu_2Zn_2 mutant protein.

This ensemble of data implies that once copper is bound in the copper site, the presence of an arginine in position 37 has only very localized effects on residues of the plug, possibly due to the presence of an extra positive charge that could affect the original conformation of lysine and other charged residues. On the basis of the NOEs described in the previous section, it seems reasonable that the side chain of Arg37 points away from the other positive residue Lys91, thus protruding toward loop I.

Comparison of the Zn_2Zn_2 Forms of asSOD1 and G37R asSOD1. The $^1H-^{15}N$ HSQC and NOESY−HSQC spectra Zn_2Zn_2G37R and Zn_2Zn_2asSOD1 have been acquired and assigned for the first time during the course of this research. The obtained assignments are reported in the Supporting Information (Table S1). If we apply the same threshold of 0.2 ppm for meaningful average chemical shift differences that has been used to compare the Cu_2Zn_2 derivatives, meaningful changes in chemical shift are observed between Zn_2Zn_2G37R and Zn_2Zn_2asSOD1 for the mutated residue Arg37, for the plug residue Leu38, and for Gln15. Gly10 has a chemical shift variation just below the chosen threshold (0.195 ppm). In this case Lys91 is substantially unchanged. The Zn_2Zn_2 forms of G37R and asSOD1 also have ^2J HSQC spectra that are nearly superimposable.

Comparison of the Cu_2Zn_2 and Zn_2Zn_2 asSOD1 Derivatives. Comparison of the spectra of the reconstituted Zn_2Zn_2G37RasSOD1 and Cu_2Zn_2G37RasSOD1 highlights differences in the chemical shift of backbone amides for selected residues. The observed differences for backbone amides are clustered around residues Phe45 and His46; Thr58, Ser59, and Gly61; Val119 and His120; and Asn139, Ala140, and Gly141. The largest effect is observed for residues Ala140 (1.84 ppm chemical shift difference) and Val119 (1.089 ppm). Notably, His46 and His120 are two copper ligands, and the side chain of Ala140 points toward the copper in the 3D structure of the as- and wtSOD1 protein. Thr58 and Ser59 are two polar residues also close to the copper site where they follow in sequence Cys57. Smaller but meaningful chemical shift differences were also observed for residues 83 and 86. Moreover, the shift values of the imidazoles of His46, His48, and His120, as well as those of His63, are also slightly different as a function of the metal present in that site, while those of the zinc site are unaltered. In summary, the presence of a zinc ion in the copper site has an effect on residues defining this metal binding site. It is interesting to note that this property is virtually identical in the G37R and asSOD1 derivatives.

The pattern of chemical shift differences observed in solution between the two metalation states of the protein parallels only partly the backbone rmsd between the X-ray structures of Cu_2Zn_2 and Zn_2Zn_2 SOD1, published during the course of this research (*34*). In that case, no specific deviations were observed for amino acids in the 80s and 120s area. In addition, relatively high deviations were reported for the protein segment 24−27, which are not observed to change at all in solution and are therefore most probably attributable to crystal packing effects.

NMR was also useful in shedding light on some dynamical properties of the Zn_2Zn_2 form that could not be inferred from the crystals. One example is represented by His63, whose imidazole side chain bridges copper and zinc in the copper(II) form of Cu_2Zn_2SOD1. In the copper(I) form, the bridge is broken with His63 binding only the zinc ion. In the X-ray structure of the Zn_2Zn_2SOD1, the bridge between the two metal centers is also broken, despite the fact that a +2 metal ion is present in the copper site. Consistently with this structure, the His63 Nϵ2 has a chemical shift value in solution in the $Zn(II)_2Zn(II)_2$ protein similar to that of the $Cu(I)_2Zn(II)_2$asSOD1 and EZn(II)-monomeric SOD1 derivatives, and the Hϵ2 resonance could be observed in 1D spectra tailored to the detection of the resonances of the exchangeable protons of histidines. These properties are common to Zn_2Zn_2G37RasSOD1 and Zn_2Zn_2asSOD1. In the spectra recorded at 600 MHz, the Hϵ2 resonance signal is rather broad with respect to the signals of the other histidine residues. The effect is reduced at 900 MHz, suggesting the presence of exchange phenomena for this proton.

Another important feature of the spectrum of the Zn_2Zn_2 derivatives (shared by G37R and asSOD1) is the presence of two sets of resonances for the nonmetal binding His43, whose side chain defines the cavity around the "plug" residue Leu38 and is usually in the protonated His^+ state. Only one of the two sets of resonances is present in the Cu_2Zn_2 derivative. The two sets of signals in the Zn_2Zn_2 derivatives indicate the presence of two different conformations of the histidine ring in the protonated form. The one present only in the Zn_2Zn_2 derivative has a strong pH dependence and disappears at pH 7, indicating that it probably originates from the interaction with a nearby residue that undergoes changes in its protonation state with pH. In any case, chemical shift differences are observed among corresponding signals of the side chain of His43 between G37R and asSOD1 for the set of signals present only for the Zn_2Zn_2 form. This observation implies that the presence of a charged residue in position 37 affects the conformation of the His43 imidazole ring.

Characterization of apo and E_2Zn_2G37R asSOD1. Having failed to find any major differences in the properties of the metalated forms of G37R asSOD1 and asSOD1, we turned to a comparison of the apoproteins. $^1H-^{15}N$ HSQC and monodimensional ^1H spectra were therefore acquired for the demetalated apo forms of the G37R and asSOD1.

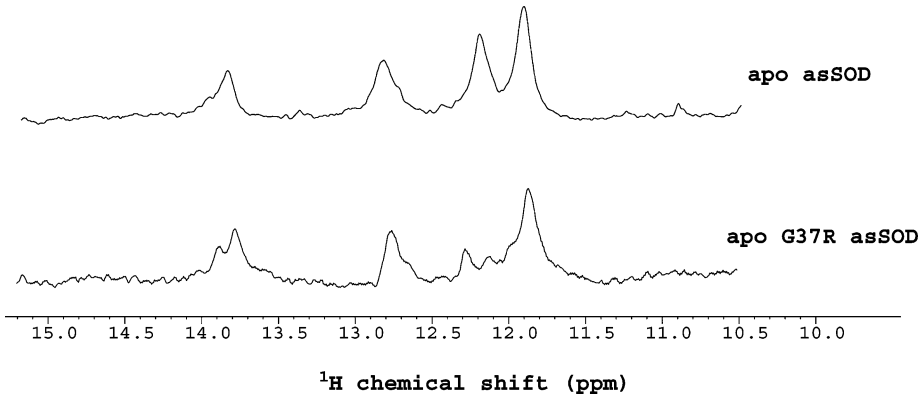

FIGURE 5: 1D ^{1}H NMR spectra tailored for the detection of imidazole NH resonances of apo asSOD1 and apo G37R.

Backbone amide resonances were assigned for apoG37R asSOD1 and apo asSOD1 using a 3D ^{1}H−^{15}N HSQC−NOESY experiment. (The assignment of apo SOD1 was only available for the monomeric form of the asSOD1 (*35*), and this assignment could not be used because we found that the chemical shift of resonances are quite different from those of the apo protein in the monomeric state). Comparison of apo G37R and apo asSOD1 revealed differences in chemical shift only for selected residues. Chemical shift differences larger than 0.05 ppm were found for residues in three different protein areas. On this basis, it appears that the mutation in position 37 affects the residues in loop I (Gly10, Asp11, Gly12, Val14, and Gly16), in loop V/strand β6 (Val94 and Ala95), and in loop III/strand β3 (Ser34, Ile35, Lys36, and Leu38).

The 1D spectra tailored for the detection of histidine NH signals are reported in Figure 5; they are very similar but not identical, indicating different conformations for the histidine side chains in the absence of metals. The difference is particularly evident for signals in the 12.0−12.5 ppm range. However, these resonances are very broad, and they were not assigned even in the apo monomeric asSOD1. Their line width is modulated by conformational exchange phenomena, and therefore they become sharper at stronger magnetic field. In ^2J HSQC spectra, signals due to the histidine residues are all clustered together, preventing a per residue assignment of these side chains.

While metalated forms of G37R asSOD1 did not show any tendency toward aggregation *in vitro*, the G37R asSOD1 apoprotein was observed to form high molecular weight aggregates as monitored by NMRD relaxation profiles. These profiles show that in solution, together with the dimeric protein, higher molecular weight species are present. The average tumbling time of the high molecular weight species varied from 150 ns in the 1-week-old sample to 430 ns on the same sample after 20 days, implying that the average size of the aggregates is on the order of 8−21 times the size of the dimeric protein. The percentage of aggregates is about 10% of the total protein in solution. Under the same conditions, apo asSOD1 formed only a small amount ($\leq$2%) of large molecular weight species, and the size of the aggregates does not show a tendency to increase with time. This tendency toward aggregation is a phenomenon that we could monitor at the relatively high concentrations typical of NMRD measurements (of the order of 3 mM).

In the case of E_2Zn_2 derivatives of G37R asSOD1 and asSOD1, once again the spectra of the dimeric proteins were different from those of the monomeric analogues. Therefore, no assignment was available for this protein form. From the monodimensional spectra tailored for the detection of the histidine protons, we have been able to establish that, while the signals of the zinc-binding histidine have the same shift in the E_2Zn_2 G37R and asSOD1, the resonances of His43 experience a clear shift, indicating that the presence of a charged residue at position 37 influences the conformation of His43. Thus, in the absence of any metal in the copper site, the plug region of E_2Zn_2G37RasSOD1 has conformational properties that are different from those of E_2Zn_2-asSOD1.

Comparisons of Protein Stabilities. We also carried out a comparison of the relative stabilities of the different protein derivatives by following the temperature dependence of the near-UV circular dichroism of asSOD1 and its G37R variant both in buffered water solutions and in the presence of variable amounts of TFE (up to 25%). The G37R protein was studied in the heterogeneous metalation state, as isolated from the expression system, as well as in the reconstituted Cu_2Zn_2 and Zn_2Zn_2 forms.

The effect of TFE as a function of temperature is reported in Figure 6. The thermal stabilities of the differently metalated forms of G37R asSOD1 were found to be nearly identical to each other and to that of Cu_2Zn_2asSOD1. In the presence of 25% TFE and temperatures higher than 50 °C, the Cu_2Zn_2asSOD1 holoprotein gave rise to a protein form with increased helical content. The same trend was observed for G37R in the heterogeneous metalation state, in the Cu_2-Zn_2 form, and in the Zn_2Zn_2 form, the latter being slightly less stable than the Cu_2Zn_2 species.

As expected, the apo form of asSOD1 was found to be less thermostable than the metalated form, and changes in its secondary structure could be observed starting at 50 °C. The apo form of G37R was also observed to be less stable than the metalated form, with changes in the CD spectrum in this case detectable starting at 45 °C.

Addition of TFE to the two apoproteins revealed dramatic differences in their secondary structure features. In the case of apo asSOD1, addition of TFE up to 25% did not significantly alter the observed behavior of the protein. In the case of apo G37R asSOD1, by contrast, addition of TFE induced a transition into a more helical structure even at room temperature. The amount of helical structure increased in a sigmoidal fashion with increasing temperature. The amount of helical content at room temperature depended strongly on the amount of TFE present, being on the order of 65%

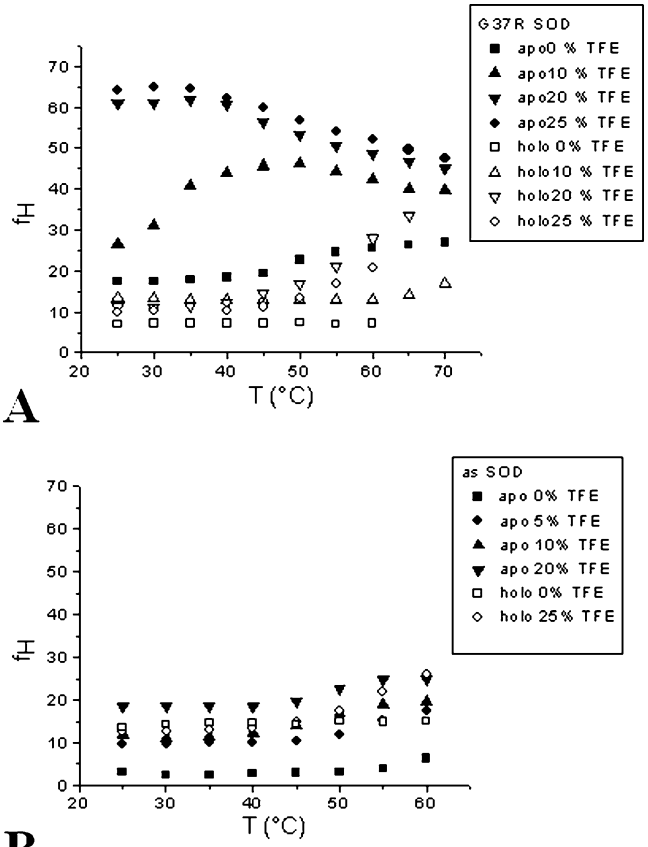

FIGURE 6: Temperature dependence of the α-helical content, f_H, derived from UV circular dichroism spectra of apo and metalated G37R (A) and asSOD1 (B) in the presence of variable amounts of TFE.

for a TFE concentration of 20% or higher. At these higher TFE concentrations, increasing temperature caused loss of secondary structure. For intermediate concentrations of TFE (e.g., 10%) the resulting profile was the sum of two different effects: a sigmoidal increase in the helical content at temperatures higher than 30 °C and a transition toward an unstructured protein form.

The observed helical forms could not be further characterized because addition even of very small amounts of TFE to the protein at the higher concentrations (0.5−1 mM) needed for extensive NMR and NMRD experiments induced severe protein precipitation.

DISCUSSION

The G37R mutation occurs in a region of the SOD1 protein that has been proposed to be critical for its stability. In particular, Leu38 has been termed the "plug" of one end of the β-barrel (Figure 1) (*36*), because it fills a cavity formed by an array of residues belonging to different β-strands: Val14 (preceding the N-terminal residue of strand β2), Ile35 (strand β3), Leu144 (strand β8), and His43 (strand β4). Notably, all these residues except Ile35 are themselves reported as fALS mutations (www.alsod.org): Leu38Val and Leu38Arg; Val14Met and Val14Gly; Leu144Ser and Leu144Phe; His43Arg.

The X-ray crystal structure of G37R human SOD1 expressed in yeast was the first published structure of a fALS-associated mutant SOD1 (*8*). In that study, the protein was expressed in yeast, demetalated to the apoprotein, and then reconstituted to its Cu_2Zn_2 form, following standard procedures. The glycine-to-arginine mutation left the protein backbone essentially unchanged in either subunit relative to wild-type.

Our NMR analysis of the conformational properties of metalated G37R in solution confirmed the X-ray findings. Small, localized chemical shift differences between corresponding metalated forms of the G37R variant and asSOD1 indicated that, consistent with X-ray, the overall protein fold is maintained between the holo forms of G37R and asSOD1. Most of the observed differences are localized in the plug area and can be related to the presence of Arg37 with a side chain pointing toward loop I; this conformation was determined by NOE patterns and is consistent with that observed in the crystal structure of the G37R mutant for the subunit with the broken His63 bridge. Moreover, all the above observations hold for both metalation states, Zn_2Zn_2 and Cu_2Zn_2, where Zn(II) and Cu(I), respectively, occupy the copper site. For both of them, a broken His63 bridge was observed. These data demonstrate that changing a glycine into an arginine at position 37 does not alter the protein structure besides very minor effects in the immediate surroundings of the mutation site. Those rearrangements could be monitored by chemical shift changes. Indeed, chemical shift is an extremely sensitive indicator of conformational rearrangements, able to reveal rearrangements that usually fall within the indetermination of NMR solution structures. Relaxation measurements indicated that the dynamical features of the G37R variant are essentially the same as those of the asSOD1. The above NMR data, together with conformational stability analysis performed by CD, lead to the conclusion that once the protein is fully metalated, the structure, the mobility, and the stability of asSOD1 and its G37R variant are substantially indistinguishable.

The situation is different if one compares the apo forms of the proteins. In the NMR spectra of apo asSOD1 and apo G37R SOD1, the chemical shift differences observed for a quite large number of residues belonging to the plug region or located at that end of the β-barrel suggest an alteration of this important feature of SOD structure in the absence of metal ions. This observation correlates with the fact that apo G37R is less stable thermally, melting at 45 °C as opposed to 52 °C for apo wt SOD1, as determined by differential scanning calorimetry (*11*) and confirmed by the present study. Major differences between the asSOD1 and the G37R asSOD1 proteins especially become apparent when TFE is added to the demetalated apoproteins. TFE is known to alter the backbone solvation of peptides and is frequently observed to induce or to stabilize α-helical conformations within those same peptides (*37*). In the case of metalated or apo wt SOD1 and metalated G37R, addition of TFE has little effect on the protein conformation. In the case of apo G37R, however, the addition of TFE causes a major conformational change resulting in an increase in α-helical content. Increasing the temperature causes the α-helical content to rise even more. We conclude that the presence of the G37R mutation has not resulted in a substantial change in the structure of the folded apoprotein in solution but instead has affected the key structural features of the plug so that (i) it melts at a temperature approximately 10 °C lower than apo asSOD1, (ii) it aggregates more rapidly than apo asSOD1, and (iii)

upon interaction with TFE it deforms into a structure with a much higher degree of α-helical content.

In seeking an explanation for SOD1-linked ALS, the challenge is to explain how such a diverse set of ALS-mutant SOD1 proteins, some of them unable to bind metals, some of them virtually unchanged from wt, and some of them severely destabilized, all cause the death of motor neurons. G37R is one of the proteins that are severely destabilized in the apo state relative to wt SOD1. Our study conclusively demonstrates that the large differences between G37R and wt are manifest only in the apoproteins and that the metalated forms are remarkably similar to each other in structure and stability. It has recently been demonstrated that even the metal-free, disulfide-intact wt SOD1 apoprotein is prone to oligomerization when incubated at 37 °C at pH 7 and that the oligomers are held together by a combination of amyloid-like, noncovalent interactions and intermolecular disulfide bridges involving Cys6 and Cys111 (*38*). We demonstrate here that even when the two above-mentioned cysteine residues are removed, as is the case for asSOD1, a tendency toward aggregation is induced by the presence of the G37R mutation. This bent for aggregation is quenched upon protein metalation. Thus the current study lends strong support to the hypothesis that it is the metal-free ALS-SOD1 apoprotein that is aggregating *in vivo*.

SUPPORTING INFORMATION AVAILABLE

^{1}H,^{15}N backbone and histidine side chain assignments for Cu_2Zn_2 and Zn_2Zn_2 metalation states of G37R asSOD1 and Zn_2Zn_2 asSOD1 and ^{15}N relaxation data measured at 600 MHz for G37R as isolated from the expression system. This material is available free of charge via the Internet at http://pubs.acs.org.

REFERENCES

1. Pasinelli, P., and Brown, R. H. (2006) Molecular biology of amyotrophic lateral sclerosis: insights from genetics, *Nat. Rev. Neurosci. 7*, 710−723.
2. Boillee, S., Vande Velde, C., and Cleveland, D. W. (2006) ALS: A disease of motor neurons and their nonneuronal neighbors, *Neuron 52*, 39−59.
3. Wang, J., Xu, G., and Borchelt, D. R. (2006) Mapping Superoxide Dismutase 1 Domains of Non-Native Interaction: Roles of Intra- and Intermolecular Disulfide Bonding in Aggregation, *J. Neurochem. 96*, 1277−1288.
4. Wang, J., Xu, G. L., Slunt, H. H., Gonzales, V., Coonfield, M., Fromholt, D., Copeland, N. G., Jenkins, N. A., and Borchelt, D. R. (2005) Coincident thresholds of mutant protein for paralytic disease and protein aggregation caused by restrictively expressed superoxide dismutase cDNA, *Neurobiol. Dis. 20*, 943−952.
5. Valentine, J. S., Doucette, P. A., and Potter, S. Z. (2005) Copper-zinc superoxide dismutase and amyotrophic lateral sclerosis, *Annu. Rev. Biochem. 74*, 563−593.
6. Elam, J. S., Taylor, A. B., Strange, R., Antonyuk, S., Doucette, P. A., Rodriguez, J. A., Hasnain, S. S., Hayward, L. J., Valentine, J. S., Yeates, T. O., and Hart, P. J. (2003) Amyloid-like filaments and water-filled nanotubes formed by SOD1 mutant proteins linked to familial ALS, *Nature Struct. Biol. 10*, 461−467.
7. Antonyuk, S., Elam, J. S., Hough, M. A., Strange, R. W., Doucette, P. A., Rodriguez, J. A., Hayward, L. J., Valentine, J. S., Hart, P. J., and Hasnain, S. S. (2005) Structural consequences of the familial amyotrophic lateral sclerosis SOD1 mutant His46Arg, *Protein Sci. 14*, 1201−1213.
8. Hart, P. J., Liu, H., Pellegrini, M., Nersissian, A. M., Gralla, E. B., Valentine, J. S., and Eisenberg, D. (1998) Subunit asymmetry in the three-dimensional structure of a human CuZnSOD mutant found in familial amyotrophic lateral sclerosis, *Protein Sci. 7*, 545−555.
9. Hough, M. A., Grossmann, J. G., Antonyuk, S. V., Strange, R. W., Doucette, P. A., Rodriguez, J. A., Whitson, L. J., Hart, P. J., Hayward, L. J., Valentine, J. S., and Hasnain, S. S. (2004) Dimer destabilization in superoxide dismutase may result in disease-causing properties: Structures of motor neuron disease mutants, *Proc. Natl. Acad. Sci. U.S.A. 101*, 5976−5981.
10. Rodriguez, J. A., Valentine, J. S., Eggers, D. K., Roe, J. A., Tiwari, A., Brown, R. H. J., and Hayward, L. J. (2002) Familial amyotrophic lateral sclerosis-associated mutations decrease the thermal stability of distinctly metallated species of human copper-zinc superoxide dismutase, *J. Biol. Chem. 277*, 15932−15937.
11. Rodriguez, J. A., Shaw, B. F., Durazo, A., Sohn, S. H., Doucette, P. A., Nersissian, A. M., Faull, K. F., Eggers, D. K., Tiwari, A., Hayward, L. J., and Valentine, J. S. (2005) Destabilization of apoprotein is insufficient to explain Cu,Zn-superoxide dismutase-linked ALS pathogenesis, *Proc. Natl. Acad. Sci. U.S.A. 102*, 10516−10521.
12. Julien, J. P., and Kriz, J. (2006) Transgenic mouse models of amyotrophic lateral sclerosis, *Biochim. Biophys. Acta 1762*, 1013−1024.
13. Wang, J., Slunt, H., Gonzales, V., Fromholt, D., Coonfield, M., Copeland, N. G., Jenkins, N. A., and Borchelt, D. R. (2003) Copper-binding-site-null SOD1 causes ALS in transgenic mice: aggregates of non-native SOD1 delineate a common feature, *Hum. Mol. Genet. 12*, 2753−2764.
14. Ferri, A., Cozzolino, M., Crosio, C., Nencini, M., Casciati, A., Gralla, E. B., Rotilio, G., Valentine, J. S., and Carri, M. T. (2006) Familial ALS-superoxide dismutases associate with mitochondria and shift their redox potentials, *Proc. Natl. Acad. Sci. U.S.A. 103*, 13860−13865.
15. Shipp, E., Cantini, F., Bertini, I., Valentine, J. S., and Banci, L. (2003) Dynamic properties of the G93A mutant of copper-zinc superoxide dismutase as detected by NMR spectroscopy: implications for the pathology of familial amyotrophic lateral sclerosis, *Biochemistry 42*, 1890−1899.
16. Banci, L., Bertini, I., D'Amelio, N., Gaggelli, E., Libralesso, E., Matecko, I., Turano, P., and Valentine, J. S. (2005) Fully metallated S134N Cu,Zn-Superoxide Dismutase displays abnormal mobility and intermolecular contacts in solution, *J. Biol. Chem. 280*, 35815−35821.
17. Hallewell, R. A., Imlay, K. C., Laria, I., Gallegos, C., Fong, N. M., Irvine, B., Cabelli, D. E., Bielski, B. H. J., Olson, P., Mullenbach, G. T., and Cousens, L. S. (1991) Thermostabilization of recombinant CuZn superoxide dismutases by replacement of free cysteines, *Biochem. Biophys. Res. Commun. 181*, 474−480.
18. Lepock, J. R., Frey, H. E., and Hallewell, R. A. (1990) Contribution of conformational stability and reversibility of unfolding to the increased thermostability of human and bovine superoxide dismutase mutated at free cysteines, *J. Biol. Chem. 265*, 21612−21618.
19. Parge, H. E., Hallewell, R. A., and Tainer, J. A. (1992) Atomic structures of wild-type and thermostable mutant recombinant human Cu,Zn superoxide dismutase, *Proc. Natl. Acad. Sci. U.S.A. 89*, 6109−6114.
20. Banci, L., Benedetto, M., Bertini, I., Del Conte, R., Piccioli, M., Richert, T., and Viezzoli, M. S. (1997) Assignment of backbone NMR resonances and secondary structural elements of a reduced monomeric mutant of copper/zinc superoxide dismutase, *Magn. Reson. Chem. 35*, 845−853.
21. Getzoff, E. D., Cabelli, D. E., Fisher, C. L., Parge, H. E., Viezzoli, M. S., Banci, L., and Hallewell, R. A. (1992) Faster Superoxide Dismutase Mutants designed by Enhancing Electrostatic Guidance, *Nature 358*, 347−351.
22. McCord, J. M., and Fridovich, I. (1969) The utility of superoxide dismutase in studying free radical reactions. I. Radicals generated by the interaction of sulfite, dimethyl sulfoxide, and oxygen, *J. Biol. Chem. 244*, 6056−6063.
23. Piotto, M., Saudek, V., and Sklenar, V. (1992) Gradient-tailored excitation for single quantum NMR spectroscopy of aqueous solutions, *J. Biomol. NMR 2*, 661−666.
24. Van Dijk, A. A., Scheek, R. M., Dijkstra, K., Wolters, G. K., and Robillard, G. T. (1992) Characterization of the protonation and hydrogen bonding state of the histidine residues in IIAmtl, a domain of the phospohenolypyruvate-dependent mannitol-specific transport protein, *Biochemistry 31*, 9063−9072.
25. Blomberg, F., Maurer, W., and Ruterjans, H. H. (1977) Nuclear Magnetic Resonance investigation of ^{15}N-labeled histidine in aqueous solution, *J. Am. Chem. Soc. 99*, 8149−8159.

26. Chen, Y.-L., Park, S., Thornburg, R. W., Tabatabai, L. B., and Kintanar, A. (1995) Structural Characterization of the Active Site of *Brucella abortus* Cu-Zn Superoxide Dismutase: A ^{15}N and ^{1}H NMR investigation, *Biochemistry 34*, 12265−12275.
27. Kay, L. E., Torchia, D. A., and Bax, A. (1989) Backbone dynamics of proteins as studied by ^{15}N inverse detected heteronuclear NMR spectroscopy: application to staphylococcal nuclease, *Biochemistry 28*, 8972−8979.
28. Palmer, A. G., III, Skelton, N. J., Chazin, W. J., Wright, P. E., and Rance, M. (1992) Suppression of the effects of cross-correlation between dipolar and anisotropic chemical shift relaxation mechanisms in the measurements of spin-spin relaxation rates, *Mol. Phys. 75*, 699−711.
29. Barbato, G., Ikura, M., Kay, L. E., Pastor, R. W., and Bax, A. (1992) Backbone dynamics of calmodulin studied by ^{15}N relaxation using inverse detected two-dimensional NMR spectroscopy; the central helix is flexible, *Biochemistry 31*, 5269−5278.
30. Kay, L. E., Nicholson, L. K., Delaglio, F., Bax, A., and Torchia, D. A. (1992) Pulse sequences for removal of the effects of cross correlation between dipolar and chemical-shift anisotropy relaxation mechanisms on the measurement of heteronuclear T_1 and T_2 values in proteins, *J. Magn. Reson. 97*, 359−375.
31. Peng, J. W., and Wagner, G. (1992) Mapping of spectral density function using heteronuclear NMR relaxation measurements, *J. Magn. Reson. 98*, 308−332.
32. Pelton, J. G., Torchia, D. A., Meadow, N. D., and Roseman, S. (1993) Tautomeric states of the active-site histidines of phosphorylated and unphospohorylated IIIglc, a signal transducing protein from Escherichia coli, using two dimesnional heteronuclear NMR techniques, *Protein Sci. 2*, 543−558.
33. Assfalg, M., Banci, L., Bertini, I., Turano, P., and Vasos, P. R. (2003) Superoxide dismutase folding/unfolding pathway: role of the metal ions in modulating structural and dynamical features, *J. Mol. Biol. 330*, 145−158.
34. Strange, R. W., Antonyuk, S. V., Hough, M. A., Doucette, P. A., Valentine, J. S., and Hasnain, S. S. (2006) Variable Metallation of Human Superoxide Dismutase: Atomic Resolution Crystal Structures of Cu−Zn, Zn−Zn and As-isolated Wild-type Enzymes, *J. Mol. Biol. 356*, 1152−1162.
35. Banci, L., Bertini, I., Cramaro, F., Del Conte, R., and Viezzoli, M. S. (2003) Solution structure of apo Cu,Zn superoxide dismutase: the role of metal ions in protein folding, *Biochemistry 42*, 9543−9553.
36. Tainer, J. A., Getzoff, E. D., Beem, K. M., Richardson, J. S., and Richardson, D. C. (1982) Determination and Analysis of 2 A Structure of Copper Zinc Superoxide Dismutase, *J. Mol. Biol. 160*, 181−217.
37. Starzyk, A., Barber-Armstrong, W., Sridharan, M., and Decatur, S. M. (2005) Spectroscopic evidence for backbone desolvation of helical peptides by 2,2,2-trifluoroethanol: An isotope-edited FTIR study, *Biochemistry 44*, 369−376.
38. Banci, L., Bertini, I., Girotto, S., Martinelli, M., Vieru, M., Whitelegge, J., Durazo, A., and Valentine, J. S. (2007) Metal-free SOD1 forms amyloid-like oligomers: a possible general mechanism for familial ALS; *Proc. Natl. Acad. Sci. U.S.A. 104*, 11263−11267.

BI700620R